Available online at www.sciencedirect.com
SCIENCE DIRECT®
C. R. Physique 5 (2004) 709–722
COMPTES RENDUS PHYSIQUE
http://france.elsevier.com/direct/COMREN/

Ice: from dislocations to icy satellites/La glace : des dislocations aux satellites de glace

Glacier flow modelling: a comparison of the Shallow Ice Approximation and the full-Stokes solution

Emmanuel Le Meur [a], Olivier Gagliardini [a], Thomas Zwinger [b], Juha Ruokolainen [b]

[a] *Laboratoire de glaciologie et géophysique de l'environnement du CNRS (associé à l'université Joseph Fourier), 54, rue Molière, BP 96, 38402 Saint Martin d'Hères, France*
[b] *Scientific Computing Ltd., P.O. Box 405, 02101 Espoo, Finland*

Presented by Guy Laval

Abstract

Several different approaches of various complexities have been used in glacier and ice sheet modelling studies. Amongst them, owing to its simplicity, the Shallow Ice Approximation appears to be the most widely adopted method. This approach, essentially used for ice sheets, owes its success to the shallow aspect of the modelled ice mass embodied in an aspect ratio ζ. When considering smaller ice bodies like alpine-type glaciers, the question arises as to whether the SIA is still valid, given that the method is all the more accurate as ζ is small. In order to test the domain of applicability of the method, results of a SIA finite difference model are compared to those of a finite element model in which the flow equations are fully considered. From a set of two-dimensional flow tests, it is shown that the accuracy of the method is much more deteriorated with increasing bedrock slopes than it is with increasing accumulation rates, even if higher accumulations lead to thicker glaciers with a larger ζ. This leads to the conclusion that when slopes become pronounced, it is a bedrock-related aspect ratio that becomes of relevance such that the bedrock slope should be the most important parameter to consider for assessing the validity of the SIA Method. A 3-dimensional simulation shows that longitudinal shear stresses explain a large part of the misfit between SIA and full-Stokes approaches. ***To cite this article: E. Le Meur et al., C. R. Physique 5 (2004).***

Résumé

Modélisation de l'écoulement des glaciers : comparaison entre l'approximation de la couche mince et les équations de Stokes complètes. De nombreuses approches, plus ou moins complexes, sont envisageables pour modéliser l'écoulement des glaciers et des calottes polaires. Parmi ces méthodes, l'approximation de la couche mince (Shallow Ice Approximation, SIA) semble être la plus utilisée, notamment pour sa grande simplicité. La SIA, essentiellement utilisée pour modéliser l'écoulement des calottes polaires, repose sur le faible rapport d'aspect ζ caractéristique de ces objets glaciaires. Pour des objets plus petits, comme les glaciers Alpins, la question de l'applicabilité de la SIA se pose puisque sa validé diminue lorsque ζ augmente. Avec comme objectif de définir le domaine de validité de cette méthode, les résultats de la SIA sont comparés à ceux obtenus en résolvant complètement les équations de Stokes à l'aide d'un code aux éléments finis. A partir de tests bidimensionnels, on montre que la solution donnée par la SIA est plus détériorée lorsque la pente du socle augmente que lorsque l'accumulation augmente, même si une augmentation de l'accumulation conduit à une augmentation de ζ. Par conséquent, lorsque la pente du socle devient importante, c'est elle qui doit être considérée, et non plus le rapport d'aspect, indiquant que la pente est donc le

E-mail addresses: lemeur@lgge.obs.ujf-grenoble.fr (E. Le Meur), gagliar@lgge.obs.ujf-grenoble.fr (O. Gagliardini), thomas.zwinger@csc.fi (Th. Zwinger), juha.ruokolainen@csc.fi (J. Ruokolainen).

1631-0705/$ – see front matter
doi:10.1016/j.crhy.2004.10.001

plus sévère des critères de validité de la SIA pour les applications glaciaires. Des simulations tridimensionnelles montrent que la non prise en compte des contraintes de cisaillement longitudinal dans la SIA contribue significativement à la différence avec la solution complète de Stokes. ***Pour citer cet article : E. Le Meur et al., C. R. Physique 5 (2004).***

Keywords: Glacier flow modelling; Shallow Ice Approximation; Stokes solution

Mots-clés : Modélisation de l'écoulement des glaciers ; Approximation de la couche mince de glace ; Solution de Stokes

1. Introduction

Over the last few decades, glaciers and ice sheets have been a subject of growing interest with ensuing numerous modelling studies implying many different types of approaches. Amongst the first models were those for large ice sheets, probably because of one characteristics in their geometry allowing for the so-called Shallow Ice Approximation (hereafter referred to as SIA, see [1]). The success of this approach comes from the possibility it offers to considerably reduce the complexity of the model equations and boundary conditions. Owing to the shallow aspect ratio (ratio of vertical to horizontal characteristic dimensions) in both the ice body and the velocity field for a large ice sheet, the SIA makes it possible to neglect some of the stress tensor horizontal gradients in the Stokes equations and similar gradients of velocity terms in the strain-velocity relations. If such a method has been abundantly used in ice sheet models, the question arises as to whether it is also applicable with smaller glaciers and under which conditions.

The SIA is based on a scale analysis of the model equations so as to be able to express them under the form of a power series of an aspect ratio ζ which expresses the shallowness of the ice body. The different levels of approximation thus depend on the level of truncation in the powers of ζ. For instance, the widely used zeroth-order model corresponds to series in which all powers of ζ higher than 0 have been discarded. Such a development in powers of ζ only makes sense if the aspect ratio is small compared to 1. This sets the limits of the method for ice geometries for which the ratio of characteristic thickness to characteristic length may become too large for the power series to have any meaning. Traditional mountain glaciers can indeed develop typical thicknesses of the same order as their width (at least locally, for instance with terminal tongues channelled into a deep and narrow valley). Some mountain glaciers, however, exhibit intermediate geometries, like cirque-type glaciers, for instance, with an overall aspect ratio still allowing for a correct expansion series. This was demonstrated by Le Meur and Vincent [2] with the Glacier de Saint Sorlin (French Alps) whose geometrical characteristics led to an ζ around 5×10^{-2}. Although it was shown that large-scale dynamics (snout position, global volume) were correctly reproduced, it appeared that the SIA was unable to model small-scale dynamics as expressed by surface velocities.

Similarly to [3], this study aims at specifying conditions required for a glacier in terms of aspect ratio and also bedrock slope in order for the SIA to apply. To this end, results from a Finite Difference model based on the SIA have been compared to those of the full-Stokes (FS) equation obtained by a Finite Element (FE) Model [4] used as a reference. The reason comes from the ability of the FE model to solve the FS equation thereby accounting for contributions from all the deviatoric stress tensor terms to the flow pattern. Here, the novel aspect comes from the fact that we have performed 3D tests and 2D tests with large bedrock slope, therefore leading to more stringent conclusions about the usability of the SIA compared to those of [3].

After the basic principles and equations of an ice flow model, the methodology of the SIA is presented with the resulting simplified set of equations it leads to. The Finite Element model is then also described. Several simulations, with different glacial conditions spanning a whole range of accumulation patterns and bedrock slopes, are then compared. Interpretation of these results allows us to list the main factors that contribute to degrading the SIA accuracy, thereby helping in indicating the domain of applicability of the method.

2. Ice flow modelling

Modelling of glaciers and ice sheets has a large range of applications. For instance, ice-sheet flow models have been extensively used for dating ice cores or for simulating the role of large ice masses on the climate system. As for mountain glaciers, it is now admitted that they represent good indicators of climate variability (IPCC [5]), since variations in their climatic environment lead to corresponding changes in their geometry and dynamics. Whatever the objectives, numerical flow models appear to be the only way of capturing the complexity of the glaciers' (or ice sheets') response to changes in their environment, a response that involves numerous processes and interactions specific to glaciers dynamics. As depicted in Fig. 1, an ice flow model consists of the expression of basic physical principles such as conservation laws (mass, momentum, energy). A specific rheology for the ice also has to be set up, as well as some initial conditions (initial ice and bedrock topographies). Boundary

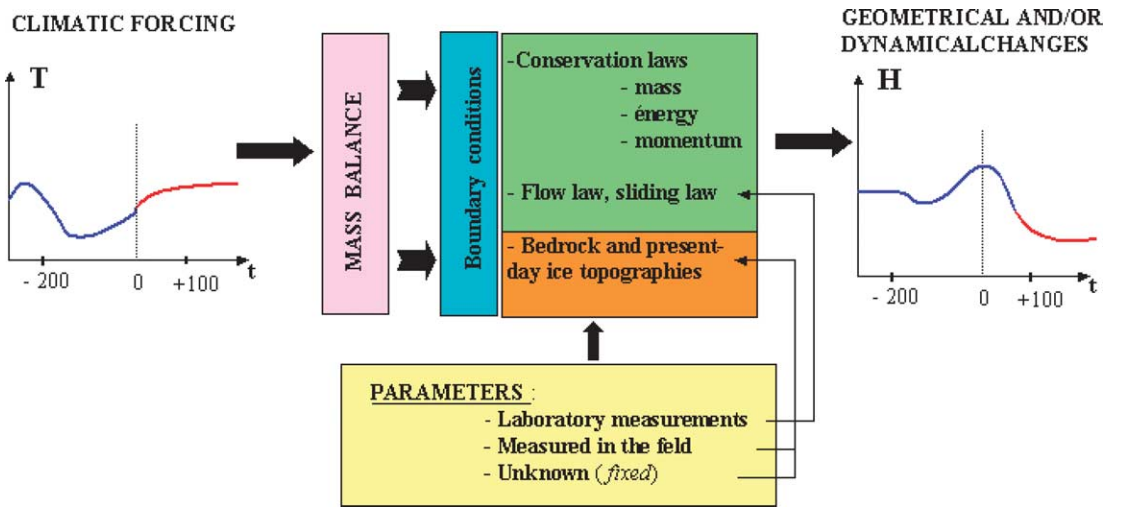

Fig. 1. Structure of an ice flow model. The highly non-linear glacier response to the climate forcing involves time lags and expresses the complexity of the problem which can only be resolved with an ice flow model. In case of a cold glacier, a temperature forcing can directly act on the ice flow by softening the ice.

conditions for the resulting equations are prescribed under various forms at the limit of the domain. For the ice/atmosphere interface, a mass balance and/or energy exchange function as well as the stress values are prescribed. However, in the simplest case of a temperate glacier, as in the present study (glacier at the melting point throughout), no energy flux needs to be taken into consideration. As for the ice/bedrock interface, the sliding velocity as well as a possible basal melting (mass exchange) are prescribed. Again, for the sake of simplicity, no basal melting is considered in the present study with bottom velocities set to zero. It should be noted that the prescribed mass balance which is either directly measured in the field or reconstructed from meteorological data (e.g., [6]) is systematically controlled by the local climate. Solving of the ensuing system of equations yields either the glacier geometrical characteristics (thickness, extent, ...) through time, or some specific fields at a given time like velocity or stress throughout the domain.

3. Ice flow equations

In an ice flow model, the different surfaces are usually expressed within a right-handed (O, x, y, z) Cartesian coordinate system as depicted in Fig. 2. The surface and bedrock Cartesian representations are defined as $z = S(x, y, t)$ and $z = B(x, y)$, respectively. In what follows, the equations governing the flow of an isothermal glacier are presented. The ice is considered as a non-linear viscous incompressible material. A more detailed derivation of the governing equations, can for instance be found in [7].

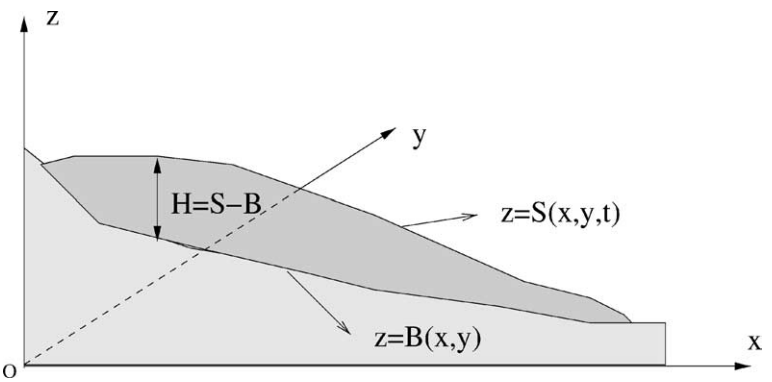

Fig. 2. Glacier surfaces expressed in a Cartesian coordinate system. Unless stated otherwise, ice thickness as used in the present study is the vertical thickness along the z direction.

Table 1
Numerical values of the parameters adopted for the simulations

$g = 9.81\ \mathrm{m\,s^{-2}}$	gravity constant
$\rho = 890\ \mathrm{kg\,m^{-3}}$	ice density for temperate glaciers
$A = 41\ \mathrm{MPa^{-3}\ a^{-1}}$	Glen's law parameter

The mass conservation equation, written here for the ice considered as incompressible, can be expressed:

$$\frac{\partial v_x}{\partial x} + \frac{\partial v_y}{\partial y} + \frac{\partial v_z}{\partial z} = 0 \tag{1}$$

with (v_x, v_y, v_z) denoting the respective x, y, z components of the velocity vector $\boldsymbol{v}$. Due to ice incompressibility, the stress tensor must be split into a deviatoric part and an isotropic pressure,

$$\tau_{ij} = \tau'_{ij} + p\delta_{ij}, \tag{2}$$

where δ_{ij} is the Kroneker symbol. Thus, the constitutive relation for the ice links deviatoric stresses to strain rates in a power law form (e.g., [8]):

$$\dot{\epsilon}_{ij} = A(T)\tau_*^2\tau'_{ij}, \tag{3}$$

where τ'_{ij} is the deviatoric stress tensor, $A(T)$ is a temperature-dependent deformation rate factor (hereafter reduced to A because of an isothermal ice body) and τ_* is the second invariant of the deviatoric stress tensor defined as:

$$\tau_*^2 = \frac{1}{2}\tau'_{ij}\tau'_{ij}. \tag{4}$$

The strain-rate components $\dot{\epsilon}_{ij}$ in (3) are linked to the velocity terms by:

$$\dot{\epsilon}_{ij} = \frac{1}{2}\left(\frac{\partial v_i}{\partial x_j} + \frac{\partial v_j}{\partial x_i}\right). \tag{5}$$

Solving for the stress terms requires expression of the force balance in the 3 directions of space leading to the Stokes equations:

$$\begin{aligned}
&\frac{\partial \tau_{xx}}{\partial x} + \frac{\partial \tau_{xy}}{\partial y} + \frac{\partial \tau_{xz}}{\partial z} = 0,\\
&\frac{\partial \tau_{xy}}{\partial x} + \frac{\partial \tau_{yy}}{\partial y} + \frac{\partial \tau_{yz}}{\partial z} = 0,\\
&\frac{\partial \tau_{xz}}{\partial x} + \frac{\partial \tau_{yz}}{\partial y} + \frac{\partial \tau_{zz}}{\partial z} = \rho g,
\end{aligned} \tag{6}$$

where g is the gravitational acceleration and ρ the glacier ice density (see Table 1).

In temperate glaciers, basal sliding also contributes to the ice motion. However, for simplicity in the present study, no sliding at the bedrock is considered ($\boldsymbol{v}(x, y, B) = 0$, where $B = B(x, y)$ is the bedrock surface). As for the free surface boundary condition, the following kinematic equation applies [7]:

$$\frac{\partial S}{\partial t} + v_x\frac{\partial S}{\partial x} + v_y\frac{\partial S}{\partial y} - v_z = a \qquad \text{for all } z = S(x, y, t), \tag{7}$$

where $z = S(x, y, t)$ is the Cartesian representation of the free surface and a the accumulation-ablation function, considered as a vertical flux. (Note that in [7], the accumulation-ablation function is supposed to be a flux normal to the free surface which explain the difference between Eq. (7) and (2.33) in [7]. From a glaciological point of view, the accumulation-ablation function has to be defined as a vertical flux.)

Reordering of all these equations finally leads to a complex system that can be reduced to 5 partial differential equations (Stokes, incompressibility and free surface equations) in 5 independent unknowns (the 3 velocity components, the isotropic pressure and the free surface elevation). In the following, assumptions and numerical methods used to solve these equations are presented for the SIA formulation as well as for the FS formulation using the FEM.

4. SIA formulation

In the following, vector components aligned with the vertical direction, are subscripted with the letter z, whereas components perpendicular to this direction are indicated with the symbol $\perp$.

Vertical integration of (1) from the ice bottom ($z = B$) to the upper free surface ($z = S$) assuming the kinematic boundary condition (7) leads to a transport equation (see, e.g., [7]):

$$\frac{\partial H}{\partial t} = a - \nabla_\perp \cdot \boldsymbol{q}_\perp, \tag{8}$$

expressing the ice thickness ($H = S - B$) rate of change as a compromise between the surface mass exchange due to the mass balance term a and the horizontal divergence of the flux. This horizontal flux $\boldsymbol{q}_\perp$ is obtained by vertical integration of the horizontal part $\boldsymbol{v}_\perp = (v_x, v_y)$ of the velocity vector over the ice thickness:

$$\boldsymbol{q}_\perp = \int_B^S \boldsymbol{v}_\perp \, \mathrm{d}z. \tag{9}$$

In Eq. (8), the operator $\nabla_\perp$ stands for the gradient evaluated in the horizontal directions, i.e. $\nabla_\perp = (\partial./\partial x, \partial./\partial y)$.

In the SIA formulation, the principle still consists of solving for the stresses (6) from which the different velocity terms are then deduced (Eqs. (3)–(5)) to finally lead to the expressions of the horizontal fluxes (9). The particularity of the approach comes from a scale analysis by which the orders of magnitude of the various variables are assessed (mainly from the peculiarities of the ice body and its environment) and serve as a basis for establishing a hierarchy of the different terms in all the intervening equations (field equations, boundary and initial conditions). Only a brief account of the SIA methodology as well as the main resulting equations are presented here. A more rigourous derivation as well as all the intermediate equations can be found in [9].

4.1. Non-dimensionalization

The first step aims at expressing each variable as the product of a typical value and a dimensionless quantity. For instance, for the 3 space variables non-dimensionalization can be expressed like:

$$(x, y) = [L](\tilde{x}, \tilde{y}); \qquad z = [H]\tilde{z} \tag{10}$$

where $[L]$ and $[H]$ are typical horizontal and vertical dimensions for the ice body (typically of the order of 10^6 m and 10^3 m respectively for an ice sheet like Antarctica for instance). The 'tilted' variables are thus dimensionless and most importantly of the order of unity. Of particular importance is the aspect ratio $\zeta = [H]/[L]$ which expresses the shallowness of the ice sheet or glacier and which will serve as the main scaling parameter for the problem. It will be seen that the smallness of ζ compared to 1 is a prerequisite for the SIA to apply since the methodology is based on a perturbation expansion under the form of series of powers of ζ. Scaling of the velocity terms follows from that of the spatial variables:

$$(v_x, v_y) = [V_L](\tilde{v}_x, \tilde{v}_y); \qquad v_z = [V_H]\tilde{v}_z \tag{11}$$

where V_L and V_H are typical horizontal and vertical velocities. It should be noted that these respective typical velocities are chosen such that the ratio $[V_H]/[V_L]$ equals the aspect ratio ζ. In other words, $[V_H]$ is only set after the respective values for $[L]$, $[H]$ and $[V_L]$ have been chosen. This is made possible because the problem exhibits a similar shallowness in the velocity field with a ratio of typical vertical to horizontal velocities of the same order as the aspect ratio ζ. Note that in some places, near the ice divide or near the bedrock if the slope is large, the proportionality between coordinates and velocities is no longer verified. Other important scalings involve the different terms of the deviatoric stress tensor and already reveal a hierarchy in their respective importance. These scalings are the result of a previous analysis [10,1] where justification for the following non-dimensionalizations can be found:

$$\begin{aligned}
&(\tau'_{xz}, \tau'_{yz}, p) = \zeta \rho g [H](\tilde{\tau}'_{xz}, \tilde{\tau}'_{xz}, \tilde{p}),\\
&(\tau'_{xx}, \tau'_{yy}, \tau'_{zz}, \tau'_{xy}) = \zeta^2 \rho g [H](\tilde{\tau}'_{xx}, \tilde{\tau}'_{yy}, \tilde{\tau}'_{zz}, \tilde{\tau}'_{xy}).
\end{aligned} \tag{12}$$

4.2. Scaled equations

Proper substitution of these new expressions into the main field equations (Eqs. (1)–(6)) yields the corresponding scaled equations. It can be easily shown that the incompressibility equation keeps a similar dimensionless form whereas the Stokes equations now becomes:

$$\begin{aligned}
&\zeta^2\frac{\partial\tilde{\tau}'_{xx}}{\partial\tilde{x}}+\frac{\partial\tilde{p}}{\partial\tilde{x}}+\zeta^2\frac{\partial\tilde{\tau}'_{xy}}{\partial\tilde{y}}+\frac{\partial\tilde{\tau}'_{xz}}{\partial\tilde{z}}=0,\\
&\zeta^2\frac{\partial\tilde{\tau}'_{xy}}{\partial\tilde{x}}+\zeta^2\frac{\partial\tilde{\tau}'_{yy}}{\partial\tilde{y}}+\frac{\partial\tilde{p}}{\partial\tilde{y}}+\frac{\partial\tilde{\tau}'_{yz}}{\partial\tilde{z}}=0,\\
&\zeta^2\frac{\partial\tilde{\tau}'_{xz}}{\partial\tilde{x}}+\zeta^2\frac{\partial\tilde{\tau}'_{yz}}{\partial\tilde{y}}+\zeta^2\frac{\partial\tilde{\tau}'_{zz}}{\partial\tilde{z}}+\frac{\partial\tilde{p}}{\partial\tilde{z}}=1.
\end{aligned}\tag{13}$$

From (4) and (12), assuming that $\tau_* = \zeta\rho g[H]\tilde{\tau}_*$, it can be shown that the non-dimensionalizated expression for τ_* is:

$$\tilde{\tau}_* = \sqrt{\tilde{\tau}'^2_{xz}+\tilde{\tau}'^2_{yz}+\frac{1}{2}\zeta^2\big(\tilde{\tau}'^2_{xx}+\tilde{\tau}'^2_{yy}+\tilde{\tau}'^2_{zz}+2\tilde{\tau}'^2_{xz}\big)}.\tag{14}$$

For the two required strain rates, assuming that $\dot{\epsilon}_{xz} = [V_L]/[H]\tilde{\dot{\epsilon}}_{xz}$ and $\dot{\epsilon}_{yz} = [V_L]/[H]\tilde{\dot{\epsilon}}_{yz}$, their respective non-dimensionalizated expressions can be expressed:

$$\tilde{\dot{\epsilon}}_{xz} = \frac{1}{2}\left(\frac{\partial\tilde{v}_x}{\partial\tilde{z}}+\zeta^2\frac{\partial\tilde{v}_z}{\partial\tilde{x}}\right);\qquad \tilde{\dot{\epsilon}}_{yz} = \frac{1}{2}\left(\frac{\partial\tilde{v}_y}{\partial\tilde{z}}+\zeta^2\frac{\partial\tilde{v}_z}{\partial\tilde{y}}\right).\tag{15}$$

4.3. Perturbation expansion

The perturbation expansion consists of expanding all field variables under the form of a power series of a small perturbation quantity, which in the present case is the aspect ratio ζ. For any scalar G, it gives:

$$G = \sum_{p=0}^{\infty} G_{(p)}\zeta^p\tag{16}$$

in which the different $G_{(p)}$ are the terms of the pth power of ζ. It is clear that the smaller the perturbation quantity, the more accurate the expansion. Then, in the scaled equations (Eqs. (13)–(15)) all variables are replaced by their corresponding power series leading to new equations in various powers of ζ. Since these equations are valid for any (assumed small) ζ, similar powers of ζ separately verify each equation such that terms of the same power of ζ can be equated. This leads to as many systems of equations as there are orders of the problem to be included.

4.4. SIA zeroth-order ice flow equations

The zeroth order system of equations is thus obtained by equating all terms $G_{(0)}$ of the zeroth power of ζ in the expanded equations, which for the Stokes equations gives:

$$\begin{aligned}
&\frac{\partial\tilde{\tau}'_{xz(0)}}{\partial\tilde{z}}+\frac{\partial\tilde{p}_{(0)}}{\tilde{x}}=0,\\
&\frac{\partial\tilde{\tau}'_{yz(0)}}{\partial\tilde{z}}+\frac{\partial\tilde{p}_{(0)}}{\tilde{y}}=0,\\
&\frac{\partial\tilde{p}_{(0)}}{\partial\tilde{z}}-1=0
\end{aligned}\tag{17}$$

and for $\tilde{\tau}_*$ and the required strain-rate expressions:

$$\tilde{\tau}^2_{*(0)} = \tilde{\tau}'^2_{xz(0)}+\tilde{\tau}'^2_{yz(0)};\qquad \tilde{\dot{\epsilon}}_{xz(0)} = \frac{1}{2}\frac{\partial\tilde{v}_{\tilde{x}(0)}}{\partial\tilde{z}};\qquad \tilde{\dot{\epsilon}}_{yz(0)} = \frac{1}{2}\frac{\partial\tilde{v}_{\tilde{y}(0)}}{\partial\tilde{z}}\tag{18}$$

where the subscript (0) refers to the zeroth order term for each variable. It can be noticed that these equations exactly correspond to the scaled Eqs. (13)–(15) in which all terms of powers of ζ would have been discarded (terms in ζ^2 in the present case). However, this is not the general rule and if it works for the zeroth order, it is due to the fact that this order only concerns constant terms. A misunderstanding sometimes emerged according to which different order-solutions would just be obtainable by equating terms of similar powers of ζ in the scaled equations. In fact, when properly solving for first-order terms (as described above) one rapidly finds that it is not so, essentially because of cross products appearing with variables raised to some powers (like, for instance, the expression for τ_*, where the terms of the zeroth-order solution appear in the higher order developments). Moreover, integration of equations of order higher than 0 requires a careful application of boundary conditions onto surfaces which are no more zeroth-order quantities, which leads to solutions already complex for the first order (implying numerous

products of zeroth- and first-order terms). In particular, from a full and rigourous derivation, Baral et al. [9] show that contrary to a general misbelief, the first order solution is not simply zero. However, the complexity of higher orders derivations is beyond the scope of this paper but their full expressions can be found in the above references. We will here restrict to the zeroth-order SIA problem as used in the forthcoming experiments.

Solution of Eqs. (17) and (18) after the variables have been made dimensionalized again by performing the inverse operation as in (10) and after dropping the subscript (0) leads to:

$$p(z) = \rho g(z - S); \qquad \boldsymbol{\tau}_{z\perp} = (\tau_{xz}, \tau_{yz}) = \rho g(z - S)\nabla_\perp S, \tag{19}$$

with $\nabla_\perp S = (\partial S/\partial x, \partial S/\partial y)$ and, after accounting for expressions for τ_* and the strain rates:

$$\frac{\partial \boldsymbol{v}_\perp}{\partial z} = -2A(\rho g)^3 (S - z)^3 |\nabla_\perp S|^2 \nabla_\perp S, \tag{20}$$

where $|\nabla_\perp S|^2 = (\partial S/\partial x)^2 + (\partial S/\partial y)^2$. Integration from $z = B$ (bedrock height) to z finally allows us to express the horizontal velocity vector $\boldsymbol{v}_\perp$ as a function of altitude z within the glacier, and surface gradient $\nabla_\perp S$. Of particular importance (see Section 6.2) is the fact that the surface velocity $\boldsymbol{v}_\perp(S)$ is proportional to the ice thickness at the fourth power according to:

$$\boldsymbol{v}_\perp(S) = \frac{A(\rho g)^3}{2} |\nabla_\perp S|^2 H^4 \nabla_\perp S. \tag{21}$$

Now making use of Eq. (9) and the general expression for $\boldsymbol{v}_\perp(z)$, the horizontal flux finally becomes:

$$\boldsymbol{q}_\perp = -\frac{2A(\rho g)^3}{5} |\nabla_\perp S|^2 H^5 \nabla_\perp S, \tag{22}$$

which once reinserted into the transport Eq. (8), yields the main SIA zeroth-order equation of the model as:

$$\frac{\partial H}{\partial t} = a + \frac{2A(\rho g)^3}{5} \left(\frac{\partial}{\partial x}\left[D \frac{\partial S}{\partial x} \right] + \frac{\partial}{\partial y}\left[D \frac{\partial S}{\partial y} \right] \right) \quad \text{with } D = H^5 |\nabla S|^2. \tag{23}$$

The above equation is then treated numerically with a semi implicit scheme (alternating-direction-implicit, see for instance [11]) after being discretized according to a finite-difference method onto a staggered regular 50×50 m grid. A more complete description of the numerical treatment as well as the complete derivation of the zeroth-order equations can be found in [9], where the SIA development is fully described.

5. Full-Stokes formulation

The numerical solution of the FS equations is obtained using the Finite Element Method based code Elmer [4]. Elmer is a multi-physics code developed at CSC, the Finnish supercomputing center in cooperation with the Helsinki University of Technology.

For the present application, both the free surface equation (7) and the Stokes equations (6) can be coupled and solved in an iterative way using an implicit scheme during the increment time step.

5.1. The free surface

Contrary to the SIA formulation, in the FEM the equations are solved in the full space and therefore the velocities of the ice on the free surface are a result of the Stokes solution (see below). The non-integrated Eq. (7) of the free surface is then solved. For brevity, Eq. (7) is rewritten in a more condensed form as

$$\frac{\partial S}{\partial t} + \boldsymbol{v}_\perp \cdot \nabla_\perp S = v_z + a. \tag{24}$$

The discrete variational form of (24) is obtained by spatial integration using the test function Φ:

$$\frac{\partial S_i}{\partial t} \int_V \Psi_i \Phi \, \mathrm{d}V + S_i \int_V \boldsymbol{v}_\perp \cdot \nabla_\perp \Psi_i \Phi \, \mathrm{d}V = \int_V (v_z + a_z) \Phi \, \mathrm{d}V. \tag{25}$$

The solution variable S has been discretized using the weight function Ψ_i:

$$S(x, y, t) = \Psi_i(x, y) S_i(t), \tag{26}$$

where S_i stands for the discrete value of S at the ith node of the discretized domain. Due to the hyperbolic nature of Eq. (25), the Galerkin method (i.e., $\Psi_i \equiv \Phi$) is not applicable. Stabilization effectively is obtained by either applying the Residual Free Bubble method [12] or the Stabilized Method [13,14].

The mesh nodes have to be re-distributed with respect to the moving boundary at the free surface. If the changes in geometry are moderate, re-distribution can be obtained by solving a linear elasticity equation for the mesh

$$\nabla\tau = 0, \quad \tau = 2\mu\epsilon + \lambda\nabla\cdot\boldsymbol{d}\cdot\boldsymbol{I}, \tag{27}$$

where $\boldsymbol{d}$ stands for the nodal displacement and $\boldsymbol{I}$ is the unit tensor. The first and the second invariant of the strain tensor are given by $\nabla\cdot\boldsymbol{d}$ and ϵ, respectively. The Lamé parameters μ and λ can be chosen arbitrarily to influence the re-distribution of the nodes. The displacements at the free surface are given in form of a Dirichlet boundary condition. The displacements at the bedrock are by definition zero since no isostasy is accounted for.

5.2. Stokes equation

The dynamics of the glacier is described by the Stokes problem for an incompressible fluid, corresponding to the solution of Eqs. (6) and (1). These two sets of equations can be re-written in a more condensed form for brevity

$$\begin{aligned} &\nabla\cdot\boldsymbol{v} = 0, \\ &-\nabla\cdot\boldsymbol{\tau}' + \nabla p = \rho\boldsymbol{g}. \end{aligned} \tag{28}$$

In (28) the deviatoric stress tensor $\boldsymbol{\tau}'$ is expressed in terms of the strain-rate tensor $\dot{\boldsymbol{\epsilon}}$ by the inversion of the power law (3). The discrete variational form of (28) is obtained by integration using the vector-like test function $\boldsymbol{\Phi}$ and the weight function Ψ_i,

$$\begin{aligned} &\boldsymbol{v}_i \int_V \nabla\Psi_i\cdot\boldsymbol{\Phi}\,\mathrm{d}V = 0, \\ &-\int_V (p_i\Psi_i - \boldsymbol{\tau}')\cdot\nabla\boldsymbol{\Phi}\,\mathrm{d}V = -\oint_{\partial V} (p_i\Psi_i - \boldsymbol{\tau}')\cdot\boldsymbol{n}\cdot\boldsymbol{\Phi}\,\mathrm{d}A + \rho\int_V \boldsymbol{g}\boldsymbol{\Phi}\,\mathrm{d}V. \end{aligned} \tag{29}$$

In the relation given above, the left-hand side term in the momentum equation given in (28) has been integrated by parts. One part is re-formulated applying Green's theorem, transforming it from an integral over the domain, V into one over the closed boundary of the domain ∂V, for which von Neumann or Newton type of boundary conditions are possible to be set (e.g., vanishing surface stress deviator components). The numerical solution of (29) in combination with (3) is obtained by either using the Stabilized Method [13,14] or the Residual Free Bubbles Method [12].

The non-Newtonian stress-strain relation introduces non-linearities into the system. Linearization of those terms implies the application of an iteration scheme. Thus, the power law given in (3) is inverted and re-formulated in terms of a quasi-Newtonian fluid with a strain-rate dependent viscosity. The variables used for evaluation of the velocity dependent viscosity for the $(n+1)$th step are taken from the previous iteration step of the algorithm. Convergence is checked upon the global change of the field variables

$$\frac{1}{N}\sum_{i=1}^{N}\left|\boldsymbol{U}_i^{n+1} - \boldsymbol{U}_i^{n}\right| < \delta \ll 1, \tag{30}$$

where $\boldsymbol{U}_i$ stands for the solution vector at the ith (out of total N) node.

6. Applications

For both the proposed 2D and 3D applications, the numerical values adopted are given in Table 1. Density corresponds to that of typical deep bubbly ice after the close off has sealed air bubbles but before their disappearance into clathrates under high pressure [15] and the Glen's law parameter follows from several studies on glacier modelling (see for instance [16,2]).

6.1. 2D applications

In order to assess the role of the bedrock slope and the accumulation distribution, we present results in the particular case of a 2D (x–z) plane-strain flow. The x-dependent geometry of the bedrock is given by:

$$B(x) = 4300 - \alpha x, \tag{31}$$

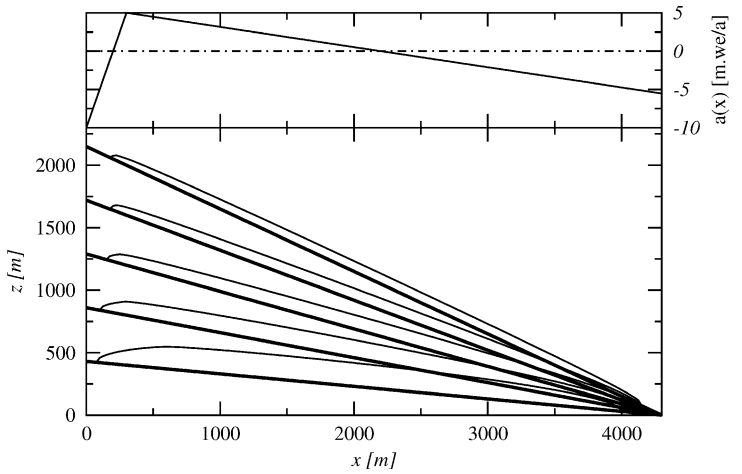

Fig. 3. Geometry of the glacier as given by the SIA formulation for the five bedrock slopes from $\alpha = 0.1$ to $\alpha = 0.5$ by steps of 0.1 and for an accumulation parameter $a_0 = 5.0$ m w.e. a^{-1} whose corresponding spatial distribution is also shown (upper part).

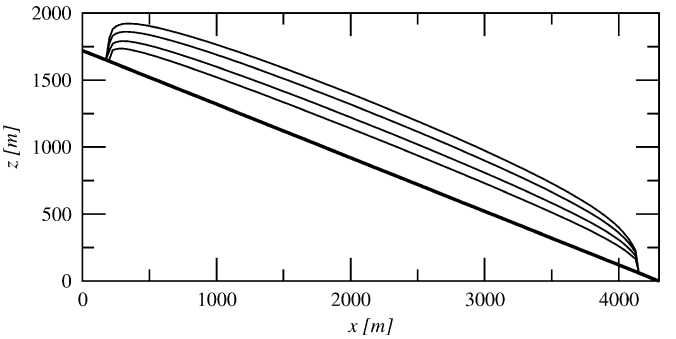

Fig. 4. Geometry of the glacier given by the SIA formulation for the four maximal accumulation $a_0 = 0.1$, $a_0 = 0.5$, $a_0 = 2.0$ and $a_0 = 5.0$ m w.e. a^{-1} and for a bedrock slope $\alpha = 0.4$. For a better reading, the ice thickness has been enlarged 5 times. The larger the a_0 value, the thicker the ice.

whereas the accumulation-ablation function (m w.e. a^{-1}), also time-constant, can be written:

$$a(x) = \begin{cases} a_0[1 - (300 - x)/100] & \text{if } x \leqslant 300, \\ a_0((2200 - x)/1900) & \text{if } x > 300. \end{cases} \tag{32}$$

The different bedrock slopes as well as the accumulation function for $a_0 = 5$ m w.e. a^{-1} are shown in Fig. 3. Tests have been carried out for slopes ranging from $\alpha = 0.1$ to $\alpha = 0.5$ by steps of 0.1, and for maximum values of the accumulation-ablation rate $a_0 = 0.1, 0.5, 2.0,$ and 5.0 m w.e. a^{-1} (see Figs. 3 and 4).

From a numerical point of view, both models have a horizontal node interval of 25 m. The mesh for the FE simulation is composed of four nodes quadrilateral elements. The mesh refinement in the vertical direction is a function of the surface elevation since the same number (20) of elements in the vertical direction is used for all the tests. To get a faster convergence, the FE simulations are started using the SIA surface elevation as an initial condition.

The influence of the two parameters, namely the maximal accumulation a_0 and the bedrock slope α are shown in Figs. 3 and 4 for the SIA simulation. As expected, the larger the accumulation, the higher the ice thickness. Conversely, the larger the bedrock slope, the thinner the glacier as a consequence of a faster flow.

All the results of the comparison are summarized in Fig. 5. As shown in Fig. 5(a), the simulations cover a range of thicknesses between $H_{\text{SIA}} = 38.3$ m to $H_{\text{SIA}} = 193.7$ m, which correspond to maximum accumulation and bedrock slope of ($a_0 = 0.1$ m w.e. a^{-1}, $\alpha = 0.5$) and ($a_0 = 5.0$ m w.e. a^{-1}, $\alpha = 0.1$) respectively. The various glacier spans (projected along the x-axis) that are all close to $L_x = 4000$ m mainly result from the adopted accumulation-ablation distribution because of the mass conservation principle. Hence, the different tests cover a range of aspect ratios $\zeta = \max(H(x))/L_x$ between 0.0097 and 0.049 (note that these aspect ratios, when calculated from ice thickness and glacier length orthogonal and parallel to the bedrock ramp respectively, give values from 1% ($\alpha = 0.1$) to 20% ($\alpha = 0.5$) smaller, which are then in the range 0.0078 to 0.048).

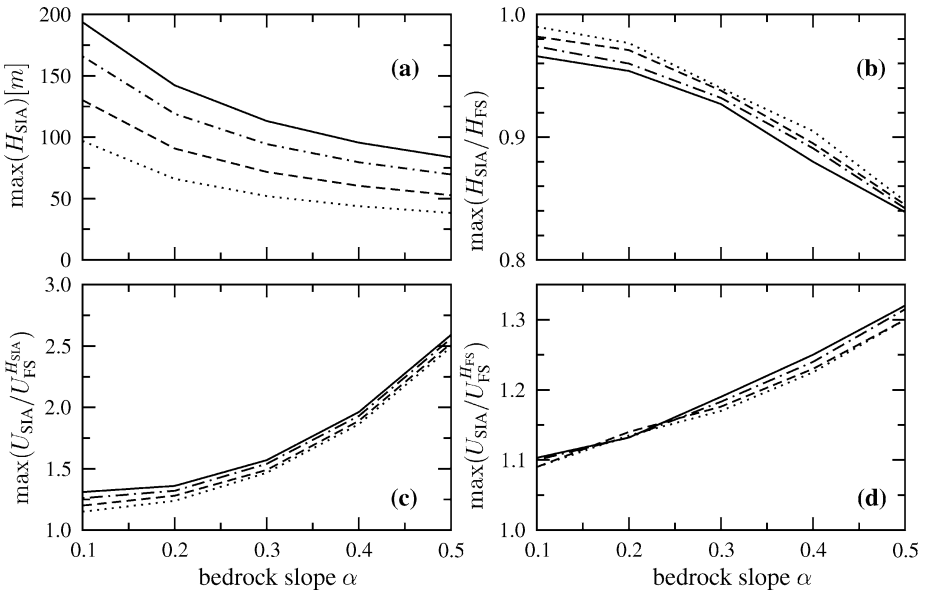

Fig. 5. Evolution as a function of the bedrock slope of: (a) the maximum ice thickness for the SIA H_{SIA}; (b) the maximum value of the SIA ice thickness to the FS ice thickness ratio $H_{\mathrm{SIA}}/H_{\mathrm{FS}}$; (c) the maximum value of the ratio of the SIA velocity U_{SIA} to the FS velocity calculated assuming the SIA free surface $U_{\mathrm{FS}}^{H_{\mathrm{SIA}}}$; and (d) the maximum value of the ratio of the SIA velocity U_{SIA} to the FS velocity calculated using the FEM free surface $U_{\mathrm{FS}}^{H_{\mathrm{FS}}}$. These quantities are plotted for different values of the maximal accumulation $a_0 = 0.1$ (doted line), $a_0 = 0.5$ (dashed line), $a_0 = 2.0$ (mixed line) and $a_0 = 5.0$ m w.e. a^{-1} (continuous line). Note that for figures (c) and (d), the vertical axes do not have the same scale.

From our results, one can see that the parameter responsible for a significant discrepancy between SIA and FS models is not the accumulation but the slope of the bedrock. Although multiplying the accumulation by a factor 50 (from 0.1 to 5.0 m w.e. a^{-1}) globally doubles the SIA ice thickness H_{SIA} as shown in Fig. 5(a), the accumulation influence on the ratio between the SIA and FS surface nevertheless remains very small (very close curves on Fig. 5(b)). Therefore these tests show that accumulation is not the crucial parameter which restricts the SIA application domain for glacier modelling. On the other hand, this ratio $H_{\mathrm{SIA}}/H_{\mathrm{FS}}$ significantly varies from 0.99 to 0.84 when the bedrock slope goes from $\alpha = 0.1$ to $\alpha = 0.5$ (Fig. 5(a)), so that the influence of the bedrock slope appears to be very pronounced. In terms of velocity Fig. 5(d) shows that the relevant velocity ratio $\max(U_{\mathrm{SIA}}/U_{\mathrm{FS}}^{H_{\mathrm{FS}}})$ significantly varies from 1.09 to 1.32 when the bedrock spans its range of variation whereas changing the accumulation parameter leads to no noticeable change (five close curves on the figure). Note that, although less significant, the $\max(U_{\mathrm{SIA}}/U_{\mathrm{FS}}^{H_{\mathrm{SIA}}})$ velocity ratio leads to very similar conclusions.

6.2. 3D application

For a classical glacier geometry, its width is generally larger than its length, so that the effects of shear stress in the horizontal plane should be not negligible. In order to access these effects, a 3D simulation is needed. The geometry of the 3D application is presented on Fig. 6 where the 3D-view of the glacier as modelled by the SIA model is depicted as well as the prescribed mass balance pattern. The potential domain of expansion for the glacier is $L_x = 4300$ m times $L_y = 3900$ m, the x-direction being the principal ice flow direction. The Cartesian bedrock equation can be expressed:

$$B(x, y) = 1000\left(1 + \frac{2(4300 - x)}{4300} - \cos\frac{2\pi y}{3900}\right) \tag{33}$$

so as to feature an inclined sine-shaped symmetrical valley with a central axis descending from 2000 m to 0 m (see Fig. 6 where only part of the domain is represented). The accumulation-ablation function has a spherical form given by:

$$a(x, y) = a_0 \frac{|R_a^2 - R^2|}{R_a^2 - R^2} \times \frac{\sqrt{|R_a^2 - R^2|}}{R_a} \tag{34}$$

where $a_0 = 1.0$ m w.e. a^{-1} and $R^2 = (1750 - x)^2 + y^2$ is the square of the distance between the maximal accumulation and the considered point, and $R_a = 600$ m is the radius of the positive accumulation area (see figure). For both models, the grid space

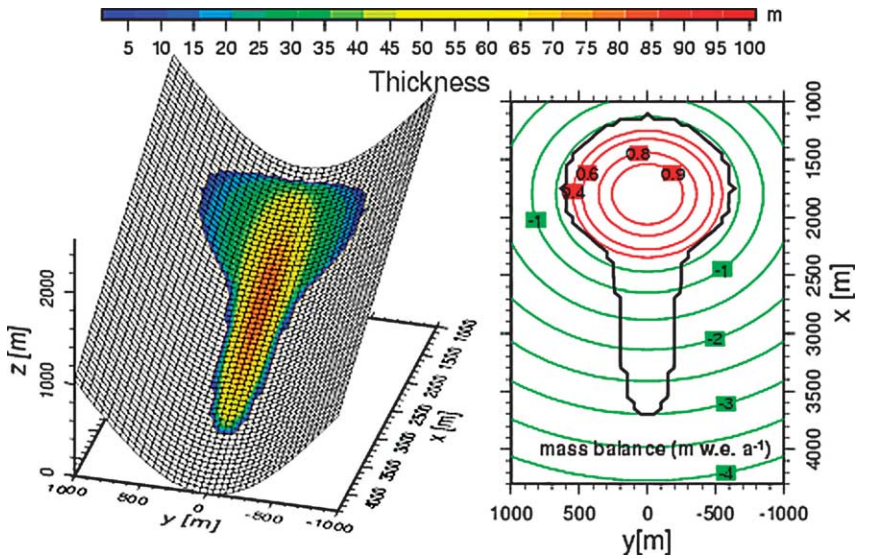

Fig. 6. 3D view of the modelled steady state glacier according to the SIA method. Also represented is the corresponding constant mass balance pattern (red curves for the accumulation zone and green curves for the abblation zone) along with the glacier outline in black.

in the horizontal plane is 50 m. For the FE simulation, the mesh is composed a given number of layers composed by eight nodes hexahedron elements. The symmetry ($y = 0$) of the model is taken into account by only meshing half the space. Moreover, since the glacier extend does not cover the whole bedrock surface, a smaller domain is adopted for the FE simulation. Then, the number of element layers in the x, y and vertical directions are 66, 15 and 20, respectively, so that the total number of elements is 19 800.

As shown on Fig. 7, the FS surface elevation is higher than the SIA one with a maximum difference of about 24 m. The lateral extent of the glacier is larger for the FS simulation than for the SIA one, and it is the reverse for the longitudinal extent. As a result, the total volume of the glacier is 97×10^6 m^3 for the FS solution and 68×10^6 m^3 for the SIA one. This difference of volume can be explain by the extent difference of the two surfaces. Contrary to the 2D flow solution, the 3D extent of the surface is not controlled only by the accumulation distribution. This difference on surface elevations can be partly explained from the difference on velocities for the two models. In the SIA, because of neglecting several stress gradients (and especially those responsible for the lateral drag along the sides of the valley) the calculated velocities are overestimated (they depend only upon the surface slope and ice thickness, see Eq. (22)). As a consequence, in order to maintain the volume flux mainly controlled by the mass balance distribution, the SIA cross-sectional area has to be smaller than that obtained for the FS solution (Fig. 7) which as a consequence, reduces the upper surface elevation.

Using the converged SIA surface elevation as an input, the corresponding velocity field can be calculated diagnostically from the FS solver of the FE code. In this case, SIA velocities are found to be 5 times larger than those given by the FS equations. However, these velocities computed on a surface that was not iteratively computed by the ELMER code in interaction with the Stokes equations are meaningless. In fact, this factor of 5 reduces to 1.9 when using more relevant velocities now obtained when the free surface calculation is coupled to the Stokes solver in the FE simulation. Considering that surface velocities are

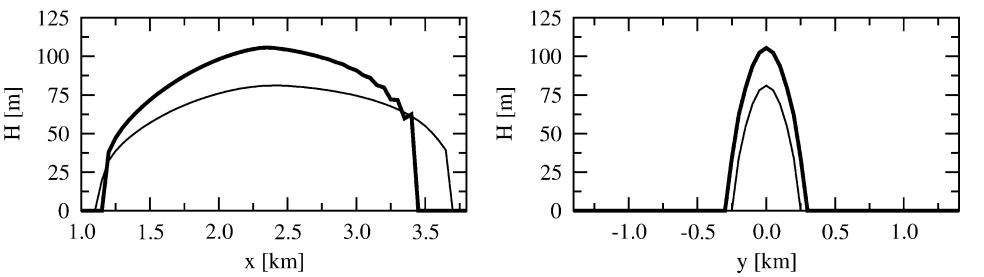

Fig. 7. SIA (thin line) and FS (bold) modelled surface elevations along the center flow line (left) and along a transverse cross section at $x = 2400$ m (right).

approximately proportional to the ice thickness at the fourth power (see Eq. (22)), it is interesting to notice that the FE velocity ratio $2.63 = 5/1.9$ between SIA and FE surfaces is similar to that of the FE to SIA surface elevation at the fourth power $(105/81)4 = 2.8$. In other words, when coupling the free surface and the Stokes equations, the higher surface elevation of the FS solution reduces the difference on the velocities between FS and SIA methods, so that the ratio actually turns to be 1.9.

A rough calculation allows us to estimate the order of magnitude of the surface value for the longitudinal shear stress τ_{xy}. By considering that the velocity v_x along the flow grows linearly from 0 at the side to a maximum value of 66 $\mathrm{m\,a^{-1}}$ at the center line at $x = 2400$ where the half width of the glacier is 250 m, the shear strain rate $\dot{\epsilon}_{xy}$ can be approximated by $1/2 \times 66/250 \approx 0.132\,\mathrm{a^{-1}}$. The corresponding longitudinal shear stress τ'_{xy} therefore can be written $(\dot{\epsilon}_{xy}/A)^{1/3} \approx 0.15$ MPa which is of the same order as the maximum value of the basal shear stress $\tau'_{yz} \approx 0.34$ MPa. It then becomes clear that neglecting this shear term in front of the supposedly predominant basal shear stress significantly contributes to the excess in velocity in the SIA formulation.

7. Discussion

The task of assessing the conditions under which an approximation procedure is valid when a more exact solution does exist may appear meaningless unless problems associated to the use of the latter arise, such as the necessary computational time. Indeed, when computing the free-surface and the associated velocity field, the SIA finite difference model required less than 1 min CPU time whereas the FS FEM model, departing from the SIA surface, still needed about 2 hours. The ratio becomes even bigger with the 3D simulation when the coupled free surface and Stokes equations had to be iteratively solved for about 4 days whilst the SIA model only required 2 min. It is therefore clear that for most glacier modelling studies, approximate approaches are still of much interest and the question of their domain of applicability remains, especially for time-dependent transient simulations where the glacier geometrical changes are studied over a long period.

As can be seen from the zeroth-order Eqs. (17), the main consequence of the SIA is to neglect horizontal stress gradients. Amongst them is the lateral shearing in horizontal planes (τ'_{xy}) whose role can be important for valley glaciers undergoing strong shearing along the side walls of the valley (as partly demonstrated by the small estimation in Section 6.2 where τ_{xy} appears to be of the same order as for the basal shear stress). The 3D simulation shows that by not accounting for this lateral drag, the SIA flow is not held back, leading to a faster flowing glacier extending farther and with a smaller average cross sectional area compared to its FS counterpart. The resulting difference in the upper free surface is of the order of 15 to 20% on the average whereas a factor of about 2 is observed between the relevant surface velocities. This result is nevertheless expectable when it becomes clear that for a glacier, large-scale changes are mostly controlled by the mass balance pattern and not so much by the details of the dynamics (e.g., [2,3]). In other words, at any place along the flow, the smaller the cross section area, the higher the flow velocities in order to maintain the ice flux essentially controlled by the mass balance distribution upstream. Inspection of the two cross sections of Fig. 7 shows that there is a factor of about 1.5 in the cross-sectional surface areas computed by both models, which then partly explains the observed high velocity ratio of 1.9. However, these results cannot be considered as entirely satisfactory because of a noticeable difference between the two modelled glaciers, a similar result as that in [3] in which their smallest glacier (close to our with a length of 1.6 km and an average slope of 0.48) also shows a similar discrepancy when modelled with the SIA and compared to its FS equivalent.

By carrying out 2D simulations, the lateral drag effect does not play anymore and it becomes possible to concentrate on others aspects like the accumulation distribution and the bedrock slope. First, for a given slope, increasing the accumulation values leads to higher aspect ratios but surprisingly does not significantly deteriorate the SIA performance. Conversely, for a given accumulation, increasing the slopes rapidly make the SIA results deviate from those of the FS model. Because it is based on a perturbation expansion (Eq. (16)) the SIA is all the more accurate as the aspect ratio ζ is small which therefore means that a topography-related aspect ratio takes over the 'classical' one when the slope increases. This point was already addressed in [10] where the SIA equations were expanded in power series of a slope aspect ratio and led to a similar theory. Therefore, the main point as clearly suggested by Fig. 5 is that the slope is the most stringent criterion for the applicability of the SIA, and that for slopes smaller than 0.2, the SIA results can still be considered as acceptable especially when accumulation remains low with as small as possible the 'classical' aspect ratio.

The discrepancy in our 3D model as well as that for the smallest glacier in [3] can also certainly be explained by their bedrock slopes (0.46 and 0.48 respectively). However, the main difference with the 2D simulation is the restricted width of the glacier (as can be seen in Fig. 7) in comparison to its length which certainly leads to a high aspect ratio and therefore reduces the accuracy of the SIA method. Nevertheless, the fact that for similar bed slopes, the modelled SIA to FS velocity ratio ($\max(U_{\mathrm{SIA}}/U_{\mathrm{FS}}^{H_{\mathrm{FS}}})$ as in Fig. 5(d)) goes from 1.3 in the 2D case to about 1.9 in the 3D case tends to indicate that the lateral drag accounts for a significant part of the total error.

It is worth pointing that all these simulations considered very simple basal conditions with bedrock flat geometries (no irregularities) and no sliding. On the other hand, it was shown that bedrock bumps, by locally transmitting longitudinal stresses

over distances of the order of several times the ice thickness [17] can locally change the flow pattern which seriously undermines the validity of the SIA. This is expressed by the fact that in such a case, the relevant aspect ratio becomes a topography related one $\zeta_N = [H]/\lambda_N$, with λ_N the smallest bedrock undulation that can be resolved with the model discretization, and which can rapidly become larger than the 'classical' one ζ (see [9]). Moreover, Hindmarsh [18,19] showed the necessity for a high basal traction for the SIA to apply, a statement confirmed by Gudmundsson [20] according to whom longitudinal stresses become important when basal traction is small like when basal sliding occurs. Thus, by neglecting basal sliding, conditions are made favourable for the SIA although such an assumption along with that of a flat bedrock is not very realistic for most alpine-type temperate glaciers.

8. Conclusion

Exclusively considering the aspect ratio as defined the usual way (ratio of typical thickness to characteristic length for the ice body) can be misleading in assessing the validity of the SIA. In 2-dimensional simulations, increasing the aspect ratio with higher accumulation rates does not deteriorate the accuracy of the method as long as the bedrock slope remains small. Conversely, increasing the bedrock slope with an aspect ratio kept small rapidly make the SIA results diverge from the full Stokes ones. A new aspect ratio related to the slope as in [9] is then more appropriate in assessing the SIA domain of application. Therefore, it seems that unless the modelled 2D glacier has a maximum thickness of the same order as its span, bedrock slopes up to 0.2 should still allow for a good SIA representation. Unfortunately, apart from ice sheets, mountain glaciers that can be represented by such 2D approaches are rare (plateau glaciers, large ice fields) and most alpine-type glaciers exhibit a strong 3-dimensional aspect. The main consequence is the role of the resulting lateral effects via the longitudinal shear stresses. However, these shear gradients effects are all the more pronounced as the geometrical aspect ratio increases with a reduced glacier width and or a larger thickness. It confirms that 3D modelling attempts still require small enough an aspect ratio as was already stated in [2] and that valley glaciers experiencing large lateral drag are problematic with the SIA. The slope effect could not be properly assessed because of computational requirements, but it is clear that the SIA will perform worse if the glaciers are steep. Therefore, steep hanging glaciers as well as tongue glaciers in deep and narrow valleys are not appropriate for an SIA modelling and should require methods solving the full Stokes equations, should the computational costs be affordable. Conversely, rather large glaciers possibly not too thick and with relatively free edges do exist (cirque glaciers, piedmont glaciers) and quite a few of them are resting on gentle slopes of less than 0.2 (see for instance [21]). For such glaciers, provided the effects of basal properties (sliding, bedrock roughness) are not too pronounced, an SIA approach can be envisaged.

References

[1] K. Hutter, Theoretical Glaciology: Material Science of Ice and the Mechanics of Glaciers and Ice Sheets, Reidel, Dordrecht, The Netherlands, 1983, 510 pp.
[2] E. Le Meur, C. Vincent, A two-dimensional shallow ice flow model of glacier de Saint Sorlin, France, J. Glaciology 49 (167) (2003) 527–538.
[3] G.J.-M.C. Leysinger Vieli, G.H. Gudmundsson, On estimating length fluctuations of glaciers caused by changes in climatic forcing, J. Geophys. Res. 109 (F1) (2004) F01007.
[4] URL: http://www.csc.fi//elmer.
[5] IPCC: Climate Change 2001, Contribution of working group I to the Third Assessement Report of the Intergovernmental Panel of Climate Change, Cambridge University Press.
[6] C. Vincent, M. Vallon, Meteorological controls on glacier mass balance: empirical relations suggested by measurements on glacier de Sarennes, France, J. Glaciology 43 (143) (1997) 131–137.
[7] R. Greve, A continuum-mechanical formulation for shallow polythermal ice sheets, Philos. Trans. Roy. Soc. London A 355 (1997) 921–974.
[8] J.W. Glen, The creep of polycrystalline ice, Proc. Roy. Soc. London, Ser. A 228 (1175) (1955) 519–538.
[9] R.B. Baral, K. Hutter, R. Greve, Asymptotic theories of large-scale motion, temperature, and moisture distribution in land-based polythermal ice sheets: a critical review and new developments, Appl. Mech. Rev. 54 (3) (2001) 215–256.
[10] L.W. Morland, Thermo-mechanical balance of ice sheet flows, J. Geophys. Astrophys. Fluid Dyn. 29 (1984) 237–266.
[11] P. Huybrechts, The Antarctic ice sheet and environmental changes: a three-dimensional modelling study, in: Ber Polarforsh, vol. 99, Alfred Wegener Institute for Polar and Marine Research, Bremerhaven, Germany, 1992, p. 241.
[12] C. Baiocchi, F. Brezzi, L.P. Franca, Virtual bubbles and the Galerkin least squares method, Comput. Methods Appl. Mech. Engrg. 105 (1993) 125–141.
[13] L.P. Franca, S.L. Frey, T.J.R. Hughes, Stabilized finite element methods: I. Application to the advective-diffusive model, Comput. Methods Appl. Mech. Engrg. 95 (1992) 253–276.
[14] L.P. Franca, S.L. Frey, Stabilized finite element methods: II. The incompressible Navier–Stokes equations, Comput. Methods Appl. Mech. Engrg. 99 (1992) 209–233.

[15] W.S.B. Paterson, The Physics of Glaciers, third ed., Elsevier, Oxford, 1994, 480 p.
[16] C. Vincent, M. Vallon, L. Reynaud, E. Le Meur, Dynamic behaviour analysis of glacier de Saint Sorlin, France, from 40 years of observations, 1957–97, J. Glaciology 46 (154) (2000) 499–506.
[17] B. Kamb, K.A. Echelmeyer, Stress-gradient coupling in glacier flow: I. Longitudinal averaging of the influence of ice thickness and surface slope, J. Glaciology 32 (211) (1986) 267–284.
[18] R.C.A. Hindmarsh, Qualitative dynamics of marine ice sheets, in: W.R. Peltier (Ed.), Ice in the Climate System, in: NATO ASI Ser. I: Global Environmental Change, vol. 12, Springer-Verlag, Berlin, 1993, pp. 67–99.
[19] R.C.A. Hindmarsh, Stability of ice rises and uncoupled marine ice sheets, Ann. Glaciology 23 (1996) 105–115.
[20] G.H. Gudmundsson, Transmission of basal variability to a glacier surface, J. Geophys. Res. Ser. B 108 (5) (2003), 9-1–9-19.
[21] Cemagref, Atlas des glaciers à risques, inventaire et suivi, Publication Cemagref, 1999.